A Comparison of Lidar Data and Two-Dimensional Simulation of Dust Transport from the Eruption of El Chichón

GUIDO VISCONTI, MARCO VERDECCHIA AND GIOVANNI PITARI

Dipartimento di Fisica, Università degli Studi, L'Aquila, Italy

(Manuscript received 2 March 1987, in final form 14 October 1987)

ABSTRACT

A two-dimensional model has been integrated for two years to study the evolution of the El Chichón aerosol cloud in the stratosphere, starting about three months after the eruption. Initial conditions for the backscattering ratios are taken from airborne lidar measurements, while observations taken at Mauna Loa are used to estimate the initial size distribution for the aerosols. Aerosols have been treated as a passive tracer, because the small changes in the stratospheric dynamics due to the aerosol interaction with solar and longwave radiation can only induce marginal effects on large scale transport. We have also completely neglected microphysical processes like coagulation as well as photochemical effects on chemically reacting species. Results are shown for aerosol extinction mixing ratios, optical thickness, mass column density and size distribution. Extensive comparison with available lidar measurements are also presented and discussed. Major discrepancies are noted between the measured optical thickness and the one predicted by the model with the former being systematically higher. Neglect of coagulation and nucleation prevents formation of large particles at high altitude which are depleted in the simulation by sedimentation. The interhemispheric asymmetry is overestimated by the model with much more aerosol being transported in the Northern Hemisphere than in the Southern Hemisphere. Other differences are found in the sudden changes in the aerosol distribution. It is argued that two dimensional models are not suitable to simulate sporadic events and that microphysics should be taken into account even several months after the eruption.

1. Introduction

The eruption of El Chichón (April 1982) has injected a considerable amount of dust into the stratosphere. The very interesting aspect of this event is that a relevant quantity of data have been collected both from ground measurements and satellites.

This collection of data represents an almost unique opportunity to test several aspects of the present knowledge of the middle atmosphere or to improve it. In particular, the study of heterogeneous chemical processes, climatic and radiative perturbations should benefit.

The problem of stratospheric aerosol interaction with radiation has been studied, for example, by Pollack et al. (1976) and Pollack and Ackerman (1983). On the other hand, the problem of aerosol droplet formation from sulfur gases injected in the stratosphere has been treated by Turco et al. (1983) with a 1D model dealing mainly with the microphysics. Pitari and Visconti (1981) and Capone et al. (1983), using a 2D model, gave more emphasis to transport. These two last modeling efforts suffered, however, from the classical Eulerian formulation of advective processes which correspond to use a rather empirical way to solve the eddy transport. The approximation is particularly weak in the case of sporadic events like volcanic clouds.

In the present work we treat the dust as a passive tracer. This means that the numerical study is started a few months after the eruption when we can assume that heterogeneous conversion of gas to aerosol particles is completed and that we ignore any interaction of dust with the radiative field. This assumption may seem particularly weak, and generally speaking it is so, but it can be justified at least for the dynamical aspect because, in the case of El Chichón, the optical thickness produced by the dust is such not to perturb, in an appreciable way, the stratospheric dynamics. However, microphysical processes which may lead to modification of the size distribution could still be active after several months.

The main purpose of this work is to use a two-dimensional model based on the residual circulation formalism to calculate the aerosol distribution as a function of time and compare it with the large amount of data collected for the El Chichón eruption (Labitzke et al., 1983; McCormick et al., 1984; D'Altorio and Visconti, 1984). This approach suffers from a number of shortcomings, the more serious being the impossibility to model any zonal asymmetry in the dust distribution. We compare our model results with lidar measurements taken in particular periods of the years

Corresponding author address: Dr. Guido Visconti, Università dell'Aquila, Dipartimento di Fisica, 67100 L'Aquila, Italy.

1982 and 1983. The dust distribution, in principle, may be determined by sporadic events (breaking of planetary waves, warmings, etc.) that cannot be intrinsically reproduced by our model. On the other hand, this kind of comparison could be useful to assess the accuracy of the schemes used at the present time to study transport in the stratosphere (i.e., residual circulation vs eulerian two-dimensional models).

Finally we note that this study represents, in any case, an improvement on previous two dimensional simulations on aerosol transport because of the most meaningful scheme adopted for parameterization of the transport itself.

2. Description of the model

The numerical experiment has been carried out using a zonally averaged model; aerosol transport is modeled in the framework of the residual circulation formalism. The residual advection (v^*, w^*) is obtained from consistent data of temperature and diabatic heating taken from the numerical output of an updated run of the stratospheric GCM of Cunnold et al. [1975, referred as MIT–GIT (Georgia Institute of Technology) from now on]. For the details concerning the dynamics and the forcing mechanisms in the 3D model we refer to the original paper of Cunnold et al. (1975). This reference can also be used for details about the choice of the model vertical levels, along with all the fixed globally averaged quantities (standard temperature and static stability in particular).

The eddy flux divergence is parameterized in terms of a diffusion tensor that can be obtained by a linear combination of a symmetric tensor representing the real dispersive effects of the eddies, and an antisymmetric tensor, representing a small correction to the meridional advection (Holton, 1981). The diffusion tensors are calculated as suggested by Tung (1983) diagnosing the eddy fields of streamfunction and vertical velocity from the same numerical output of the MIT–GIT stratospheric GCM. We have made some improvements in the 3D model with respect to the original version in connection with the forcing mechanism in the lower stratosphere (ozone heating in the 9.6 μ band and refinements in the parameterized formula for the exchange of latent and sensible heat). The approach we have adopted here for the two-dimensional model has been extensively discussed in Pitari and Visconti (1985), Visconti and Pitari (1987) and Pitari et al. (1987). A more general discussion on this problem can be found in Plumb (1987). Until now, two basic approaches have been used to derive the eddy diffusion for 2D models. The one illustrated by Kida (1983) and Pitari and Visconti (1985) used the statistics from a large number of particles or direct integration of the displacement to derive K. Plumb and Mahlman (1987) have solved the problem using eddy fluxes for two independent tracers in the GFDL, 3D tracer model. The original data in Pitari and Visconti (1985) were obtained from a general circulation model of the stratosphere and that model (as in the case of Kida) did not correctly reproduce the climatology of the stratosphere. However, the K derived in this way are consistent with the residual circulation, which is also obtained as a byproduct of the GCM output. We can now illustrate, in particular, some of the shortcomings of MIT–GIT model we have used. As pointed out in Pitari and Visconti (1985) this model does not reproduce the observed wind field in the tropical region; the predicted stationary eddy contribution to the geopotential at 10 mb is also too large. Problems also exist for the temperature and ozone field in the winter polar stratosphere and for the closure of the mesospheric jet. We could expect that discrepancies of this kind would more directly affect the heating rate and then the residual circulation. A comparison has been made between the circulation calculated from the model and the monthly means (for January and March) of the residual circulation calculated from the LIMS data in Gille et al. (1987) between 100 and 0.1 mb. At the equinox the behavior of the two cells in our model is very similar to the ones calculated from LIMS. Even smaller cells between 10 and 1 mb show up in both calculations. However, in general the velocities given by the 2D model are larger up to a factor of two with respect to LIMS. In this season the spring hemisphere in the LIMS data shows a pronounced region of southward moving air between 10 and 1 mb which although present in the 2D model is much smaller. The solstice season shows the same behavior with the circulation given by the model being much faster than the observed one.

These characteristics of the dynamics of the 2D model will affect the simulation of aerosol transport. In any case, the results will give indications on the performance of the method we have used to derive these dynamical parameters and also indirectly on the overall rating of the 3D model.

The continuity equation we use for the aerosol mass mixing ratio is the following:

$$\frac{\partial \bar{\chi}(r)}{\partial t} = -\frac{1}{a\cos\phi}\frac{\partial}{\partial \phi}(\bar{v}^*\bar{\chi}(r)\cos\phi) - \frac{1}{\rho_0}\frac{\partial}{\partial Z}(\bar{w}^*\bar{\chi}(r)\rho_0) - \frac{1}{\rho_0}\frac{\partial}{\partial Z}(w_s(r)\bar{\chi}(r)\rho_0) - \nabla\cdot\mathbf{F}^*(\bar{\chi}(r)) - L\bar{\chi}(r) \quad (1)$$

with

$$\mathbf{F}^*(\bar{\chi}(r)) = -(\mathbf{K}_s + \mathbf{K}_a)\nabla\bar{\chi}(r) \quad (2)$$

where the overbar denotes a zonal average. The variables in (1) and (2) are the following:

χ aerosol mass mixing ratio
r aerosol radius

t, ϕ, a time, latitude, earth radius
Z log-pressure vertical coordinate, $-\ln(p/p_s)$
p, p_s pressure, reference pressure
v^* residual meridional velocity (positive northward)
w^* log-pressure residual vertical velocity, (positive upward)
$w_s(r)$ sedimentation velocity for dust particles of given composition
$\rho_0(Z)$ standard density profile relative to the reference density, $\rho_0(Z) = \rho_s e^{-Z}$
F^* eddy flux due to wave transience
$\mathbf{K}_s, \mathbf{K}_a$ symmetric and antisymmetric diffusion tensors
L washout rate

The residual velocities are calculated as described by Dunkerton (1978), but retain the temperature advection in the meridional plane and the local temperature changes (Solomon et al., 1986):

$$\bar{w}^* = \frac{\bar{Q} - \partial\bar{T}/\partial t - \bar{v}^*/a\partial\bar{T}/\partial\phi}{\tilde{\sigma}} \quad (3)$$

$$\frac{1}{a\cos\phi}\frac{\partial}{\partial\phi}(\bar{v}^*\cos\phi) + \frac{1}{\rho_0}\frac{\partial}{\partial Z}(\bar{w}^*\rho_0) = 0 \quad (4)$$

where T is the temperature, $\tilde{\sigma}(Z)$ the globally averaged static stability and Q is the diabatic heating. Equation (4) represents the continuity equation for v^* and w^*.

Again for an overall discussion on the transport parameterization from a 3D model dataset in a "Lagrangian" formalism we refer to the paper by Pitari and Visconti (1985). Apart from the mentioned improvement in the calculation of the diffusion coefficients, the main difference between the formalism used there and the one described in this paper is that the residual circulation is not seasonally averaged but is made explicitly time dependent, in order to have a more realistic treatment of the transport.

The time dependency of the residual circulation is obtained by a fit of the temperature and diabatic heating data coming from the 3D model with the following equation at each level:

$$A(t) = \tilde{A} + a_2{}^0P_2{}^0 + a_4{}^0P_4{}^0 + \sin\delta t(a_1{}^0P_1{}^0 + a_3{}^0P_3{}^0) \quad (5)$$

where A is a general zonally averaged quantity, $P_n{}^0$ are the associated Legendre polynomials with $m = 0$, $a_n{}^0$ are the resulting time-series coefficients. In the seasonal sine wave t is zero at the March equinox and δ is (2π/one year). The tilde denotes a global average over an isobaric surface. The same approach has been used for the $\mathbf{K}$ components in the eddy flux divergence expression.

We stress, at this point, that the dust has been treated here as a passive tracer and no attempt is made in this work to see how the stratospheric dynamics could be influenced by the dust interaction with solar and infrared radiation. In a companion paper devoted explicitly to studying these dynamical effects (Pitari et al., 1987) we show how the large scale transport is only marginally affected by the presence of the El Chichón aerosols. These arguments only apply to large scale transport of nonreacting species, while chemically reacting species could certainly be affected by photochemical effects due to the presence of dust and sulfur compounds in the stratosphere (the latter lasting only for few months after the eruption).

Equation (1) is solved at the same vertical levels of the original 3D model from pole to pole with a 10° latitude resolution. Boundary conditions are zero lateral fluxes at the poles, while in the vertical we assume the aerosol distributed with a scale height determined by rainout at the ground and by sedimentation at the top. Top height for $\bar{\chi}(r)$ is fixed well below the model top, depending on the $w_s(r)$ magnitude.

The choice of the initial size distribution for the aerosols and its time evolution is discussed in the following section, along with the design of our numerical experiment in time following the El Chichón aerosol cloud.

3. Aerosol size distribution

Our numerical experiment starts on 10 July 1982, about three months after the eruption. At this moment we can assume that the conversion of sulfur gases to aerosol particles in the stratosphere (that is a complex problem by itself) is completed. From now on, all the microphysical processes acting on the aerosol (coagulation, condensation, etc.) are neglected and the only processes determining the concentration of aerosol are advection, diffusion and sedimentation. These assumptions may be criticized especially considering the data reported by Hoffman and Rosen (1984). They show that nucleation has been active even in early 1983. Also, in these data the behavior of the size distribution show no evidence of depletion for larger size ($r \geq 0.25$ μ) as one would expect if the particles were acted upon only by sedimentation. On the other hand, the comparison with lidar data should not be affected by differences in size distribution. Pinnick et al. (1980) have shown that the backscattering coefficient is rather independent of this size distribution for sulfuric acid aerosol as long as large particles ($r > 1.6$ μ) are absent. Mid-July is chosen in order to use the backscattering ratios measured by McCormick et al. (1984) as initial data for the integration in time of Eq. (1).

Figure 1 shows, in the upper drawing, the contours of the extinction mixing ratios used as initial data; in the lower drawing we show the associate column mass density for the aerosols assuming a particle density of 1.65 g cm^{-3} that corresponds to a 75% concentration by weight of sulfuric acid in a spherical droplet. The extinction mixing ratios shown in this figure are taken

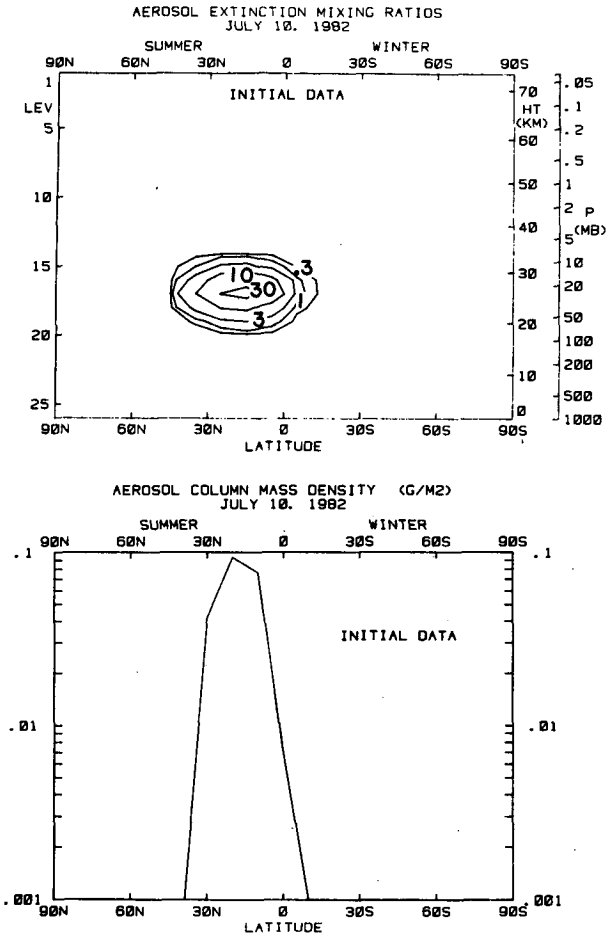

FIG. 1. Initial data for the extinction mixing ratios of the El Chichón aerosols at $\lambda = 0.6943$ μm (upper drawing). Lower drawing shows the corresponding aerosol column mass density in g m^{-2}. Both drawings refer to 10 July 1982.

at $\lambda = 0.6943$ μm. The aerosol size distribution is chosen following the measurements taken at Mauna Loa during July 1982 and reported in the paper of King et al. (1984). The reference size distribution is obtained by integrating the cumulative size distribution between 21.5 and 24.5 km:

$$\frac{dN}{d\log r} = Cr^{\nu+1}\exp(-\beta r) \qquad (6)$$

where N is the number of particles per square cm per log radius, in a vertical column and C, ν, β are distribution parameters:

$$C = 9.897 \times 10^{19}\ \text{cm}^{-2}\ \mu\text{m}^{-13.65}$$

$$\nu = 12.65$$

$$\beta = 39.3\ \mu\text{m}^{-1}.$$

The size spectrum is divided in nine size bins; radius values representative of each size are 0.01, 0.02, 0.04, 0.08, 0.16, 0.32, 0.64, 1.28, 2.56 μm. Due to the exponential decrease of concentration (and mass), we only retain five size bins (0.08, 0.16, 0.32, 0.64, 1.28 μm) in order to speed up the computer code.

Figures 2a–c show the aerosol size distribution integrated in the atmospheric volume between 30–35 km, 25–30 km and 10–15 km. In each of these figures five curves are reported corresponding to different times in the numerical experiment. We show the size distribution at the beginning of the run and its evolution every three months. The initial size distribution is taken from observation (King et al., 1984) and it is missing from Fig. 2c because no particles are detected below 15 km at that moment.

We have selected three altitude ranges corresponding to the upper and lower boundaries of the dust cloud, where the modifications of the size distribution induced by a radius-dependent particle sedimentation are more evident. We see how above 25 km the total number of particles rapidly decreases with the average radius moving toward smaller particles. This is probably due to our assumption of a uniform initial size distribution within the cloud, while Eq. (8) has been obtained by integrating between 21.5 and 24.5 km.

On the other hand, below 15 km (Fig. 2c) an increasing number of particles is found (with a maximum reached during the 1982/83 winter season) along with a predominance of larger particles.

The numerical experiment is carried out for about

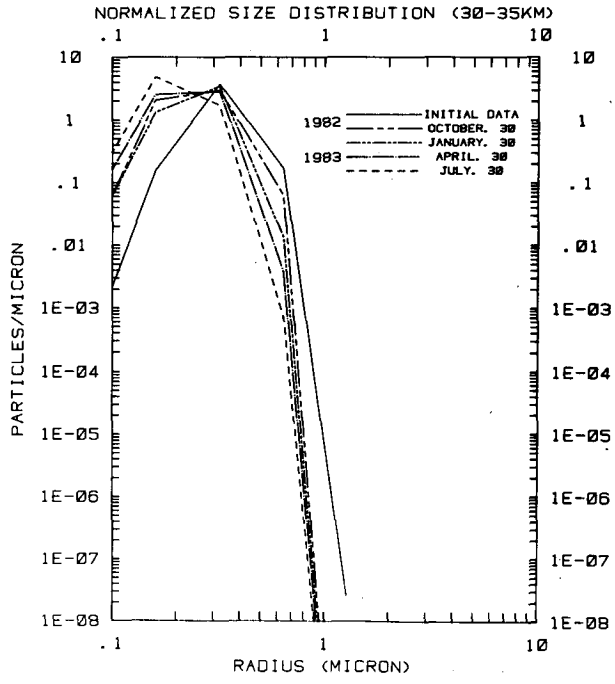

FIG. 2a. Size distribution of the El Chichón aerosols. Values are integrated in the atmospheric volume between 30 and 35 km of height. The curves refer to different periods of time as specified.

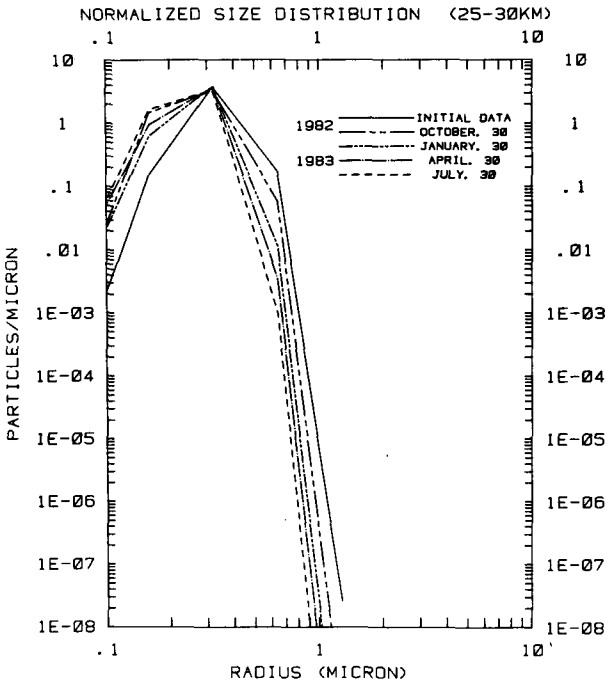

FIG. 2b. As in Fig. 2a for the atmospheric layer between 25 and 30 km.

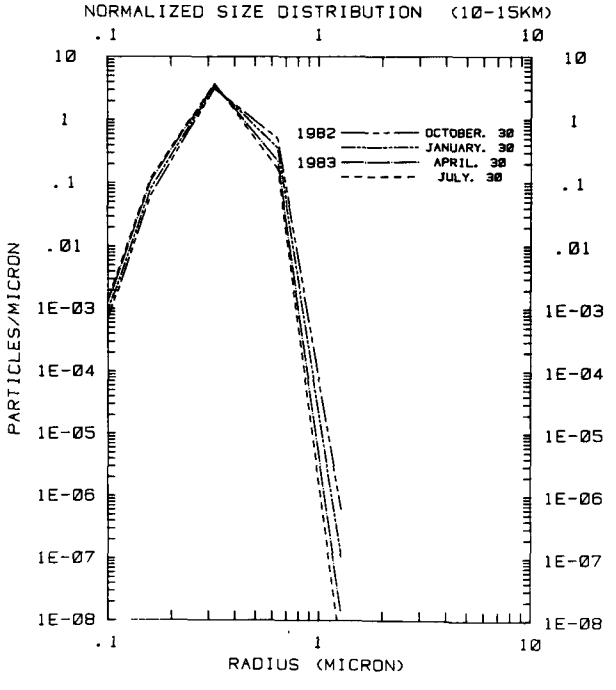

FIG. 2c. As in Fig. 2a for the atmospheric layer between 10 and 15 km.

two years, until the total mass of El Chichón aerosols in the model atmosphere is about one tenth of the initial value assumed to be 11 megatons. The latter has been taken from the work by McCormick and Swissler (1983) and it allows us to translate the initial backscattering ratios to mass mixing ratios for the aerosols. These ratios can be converted, in turn, to optical thicknesses using the conversion value for integrated backscatter to aerosol optical thickness as determined in the work by Swissler et al. (1983). The value derived was 42.8 ± 7.4 sr (steradian) for $\lambda = 0.6943$ μm.

Figure 3 shows the behavior of the total mass in the two-year integration of the model; rainout is the main loss mechanism for the aerosols when they penetrate the troposphere where they are transported by large scale motions and sedimentation. The rainout process is parameterized following the method suggested by Pitari and Visconti (1980) that consists of the calculation of a precipitation probability at each grid point depending on temperature, temperature variance and water vapor content. The rainout rate is then given by the precipitation probability divided the residence time assumed for the present case to be 2.5 days.

Equation (1) has been integrated using the N-cycle time integration scheme (Lorenz, 1971) with a three-hour time step per cycle and a total of four cycles.

4. Results and discussion

We have already mentioned above that once aerosol composition and size distribution are assumed it is possible to obtain from the backscattering ratio information about the extinction and the mass mixing ratio. In what follows we will refer to the extinction mixing ratio which is defined as

$$R(Z) - 1 = f_A(Z)/f_M(Z) \tag{7}$$

where $R(Z)$ is the backscattering ratio, $f_A(Z)$ is the

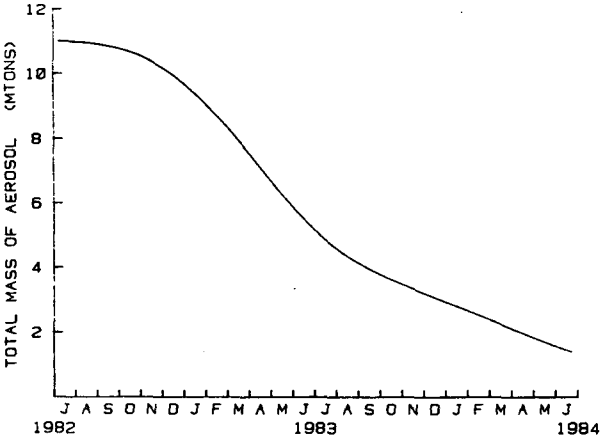

FIG. 3. Total mass of El Chichón aerosols in the model atmosphere as a function of time. Units are megatons.

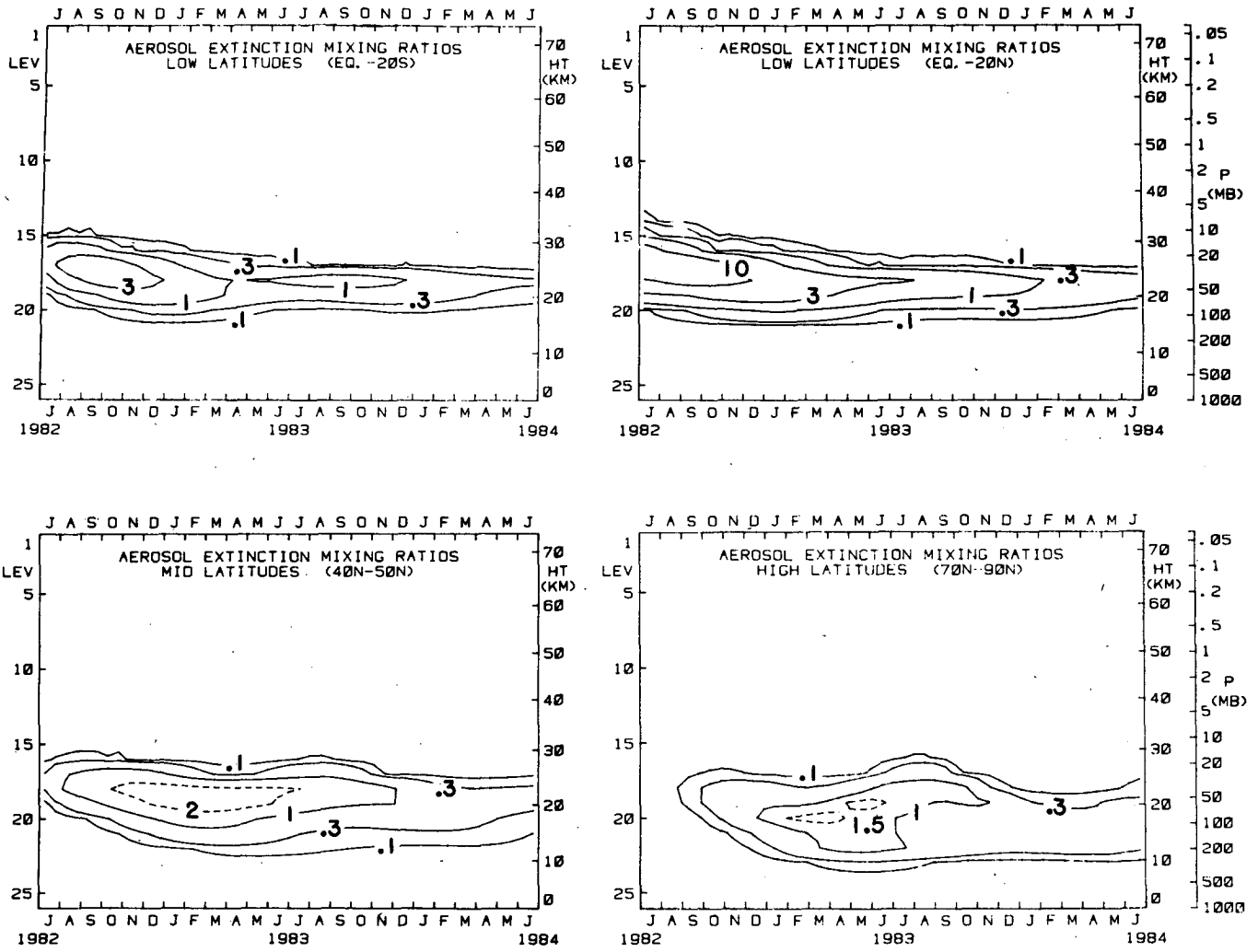

FIG. 4. Extinction mixing ratios at 0.6943 μm as a function of altitude and time. The four drawings refer to (from the upper left): low latitudes (South), low latitudes (North), midlatitudes (North), high latitudes (North).

aerosol backscattering function (km sr)$^{-1}$ and $f_M(Z)$ is the molecular backscattering function. The aerosol integrated backscattering function is given by

$$\int_{Z_1}^{Z_2} f_A(Z)dZ = \int_{Z_1}^{Z_2} (R(Z) - 1)f_M(Z)dZ \qquad (8)$$

which is measured in sr^{-1}. The aerosol backscattering function depends on the efficiency factor for backscattering (Q_{bs}) and the size distribution $n(r)$ as $f_A(Z) = \int \pi r^2 Q_{bs}(m, r/\lambda)n(r)dr$: Q_{bs} also depends on the refractive index m of the aerosol. Once f_A is known from (8), the aerosol composition and the size distribution should also set the ratio Qe/Qbs, between extinction and backscattering, so that in principle it is possible to determine the total aerosol extinction. This procedure has been followed to reduce the initial data, as mentioned in the previous paragraph. However, Pinnick et al. (1980) have shown that the assumption can be made of both backscattering and extinction, independent of size distribution. In what follows, we will compare lidar backscattering ratios at 0.55 and 0.6943 μm which will be described within the framework of the above definition and assumption.

Evolution of size distribution is given in Figs. 2a–c; because of the sedimentation process the size distribution is being depleted of the larger particles, at the least above 25 km. In the 10–15 km range there is a partial replenishment for larger size due to deposition from higher altitudes. Our results do not seem to reproduce the data very well. Hoffman and Rosen (1984) have shown that after more than a year after the eruption, aerosol concentration for particles with $r > 0.25$ μm does not change appreciably at 17 km and also larger particles do not reside necessarily at lower altitudes than smaller particles. In our case, in the 30–35 km range aerosol concentration for $r > 0.25$ μm represents about 88% of the total at the beginning and

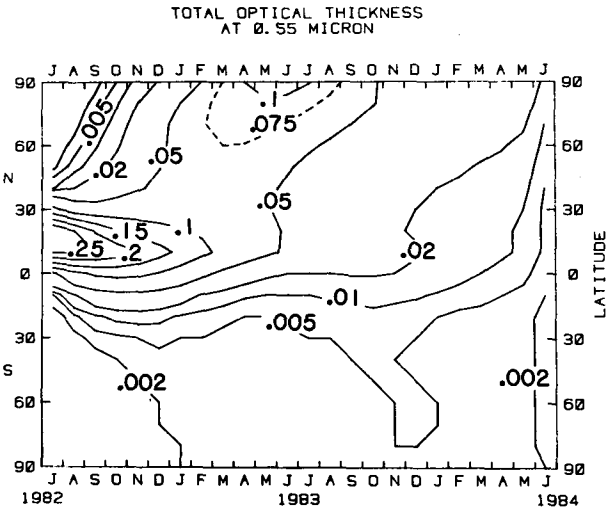

FIG. 5. Total optical thickness at 0.55 μm as a function of latitude and time.

reduces to 28% after a year. In the 25–30 km range, after a year, the same size represents 58% of the total. These results seem to indicate that at least coagulation should be taken into account.

Figure 4 shows the model results for the aerosol extinction mixing ratios. We show the evolution of the aerosol cloud with time at four different latitude bands up to two years from the beginning of the run.

In the tropics the downward and poleward motion of the aerosol with a subsequent rapid decrease of the backscattering ratio and the altitude of the peak is evident. At midlatitudes the highest ratios (~2.5) are reached about ten months after the eruption while in the arctic region the maximum (1.5) is attained two months later. As a result of the mid-high latitude subsidence we see that the cloud is moving to the lower stratosphere and the downward motion is particularly

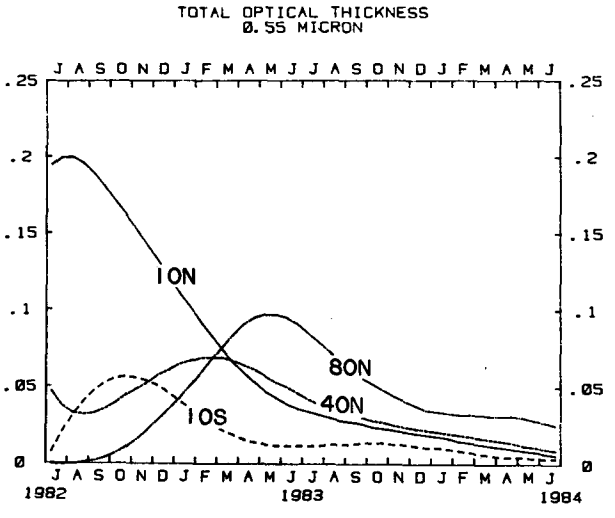

FIG. 6. As in Fig. 5 at selected latitude bands ($\Delta\phi$ = 10°).

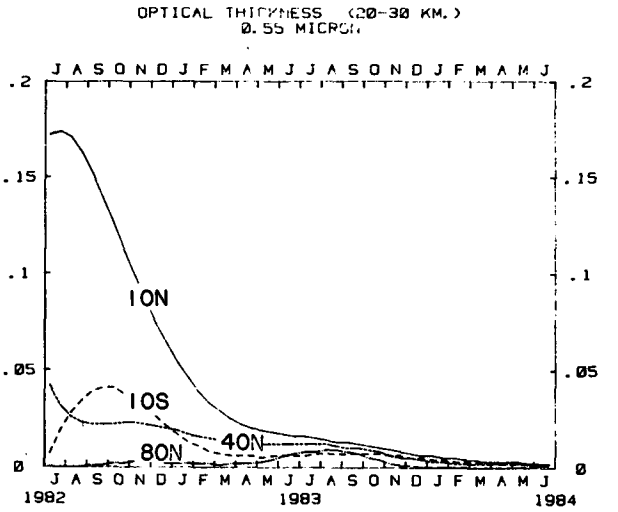

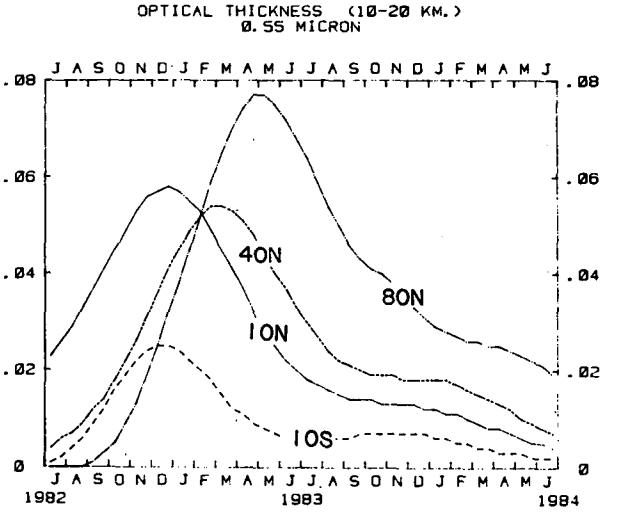

FIG. 7. Upper drawing shows the optical depth at 0.55 μm in the layer between 20 and 30 km. Lower drawing refers to the layer between 10 and 20 km. Selected latitude bands are as in Fig. 6.

fast during the winter seasons. All curves refer to a 0.6943 μm wavelength to allow a direct comparison with the lidar measurements of McCormick et al. (1984), as we will see later.

Figure 5 shows, in a latitude–time plot, the global behavior of the total optical thickness at λ = 0.55 μm (this wavelength is chosen for an easier comparison with the lidar data of D'Altorio and Visconti, 1984, as we will see later). The major features shown are the decrease with time of the tropical maximum, the shift of the total optical depth maximum from the tropics to mid and high northern latitudes and finally the negligible penetration of dust in the Southern Hemisphere. Lidar measurements have shown sporadic penetration of dust in the Northern Hemisphere since late summer and also limited transport in the Southern Hemisphere. This effect has also been shown in satellite data

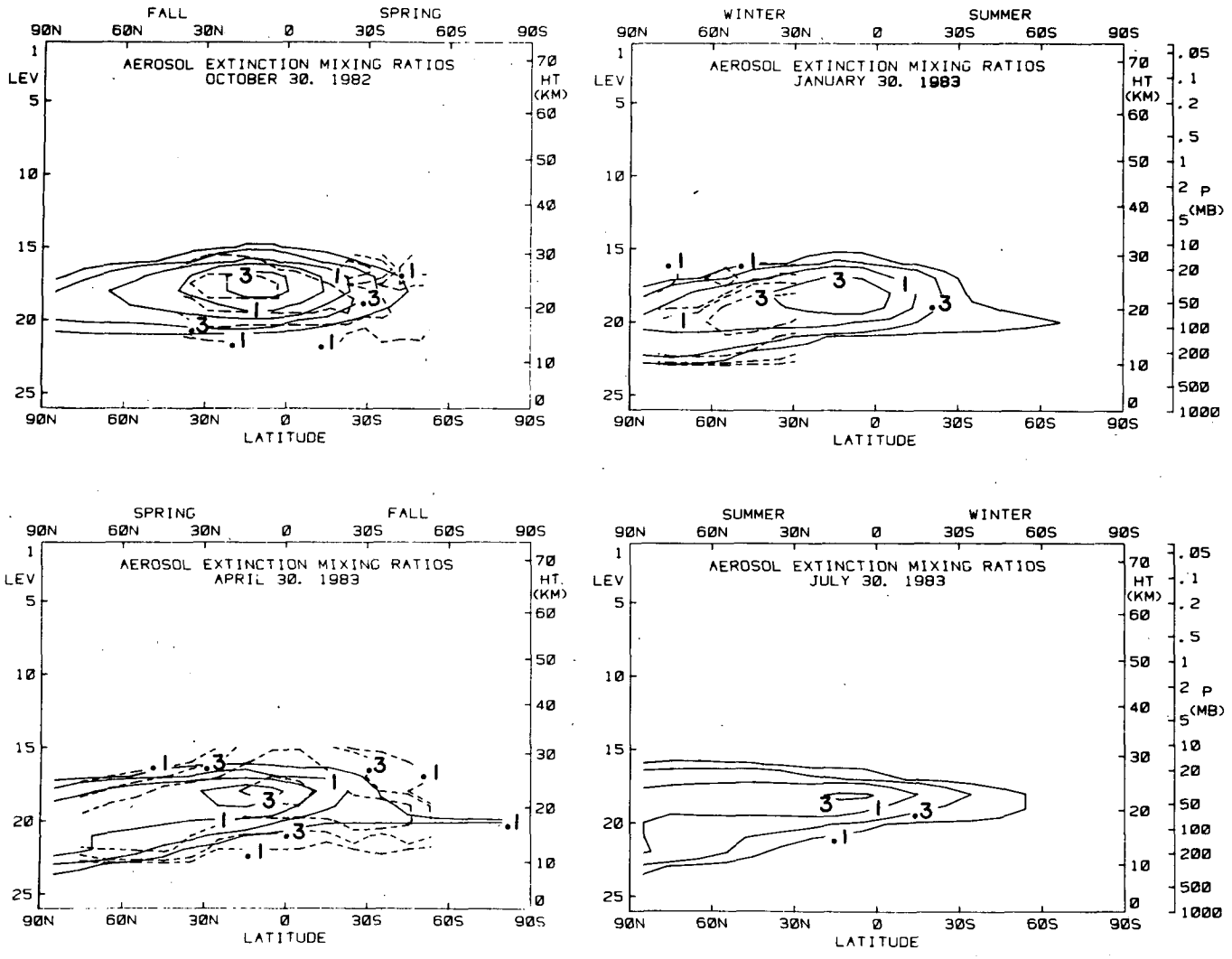

FIG. 8. Extinction mixing ratios at 0.6943 μm as a function of height and latitude. The four drawings refer to (from the upper left): 30 October 1982; 30 January 1983; 30 April 1983; 30 July 1983. Dashed lines refer to the lidar data of McCormick et al. (1984).

(McCormick, 1986) which nevertheless appears to be exaggerated in the model results. In the long run, this slower transport in the Southern Hemisphere produces an aerosol concentration in the Antarctic that is too low, so that there is an order of magnitude difference in the optical depth between Arctic and Antarctic. Recent data reported by McCormick and Trepte (1987) show that the optical depth between the two regions differ by a factor of 2.

Figure 6 represents the same data plotted in the previous figure in a different form. We show the results averaged on four latitude bands centered at 10°S, 10°N, 40°N and 80°N respectively. The same is done in Fig. 7 where we split the optical depth in two parts: contributions from high levels (20–30 km) and low levels (10–20 km). It is clearly seen how the dust moves downward as a result of the cumulative effects of sedimentation and large scale transport. The low level filling appears to happen with a delay of 8–12 months from the eruption, depending on the latitude. After this time, the tropospheric penetration rate and subsequent loss of aerosols appears to be faster than the filling from upper levels or from tropical latitudes, especially for the dust in the mid to high latitude bands. After two years a maximum value of 0.02 is found for the optical depth in the arctic region.

Figures 8 and 9 show a comparison of our model results with lidar measurements of McCormick et al. (1984). Figure 8 shows extinction mixing ratios as a function of latitude and altitude starting from 30 October 1982 and the comparison is made each three months up to July 1983. This comparison shows a general agreement, however we have to point out two important differences: the already mentioned negligible penetration of dust in the Southern Hemisphere as predicted by our model is clearly shown; we see in the

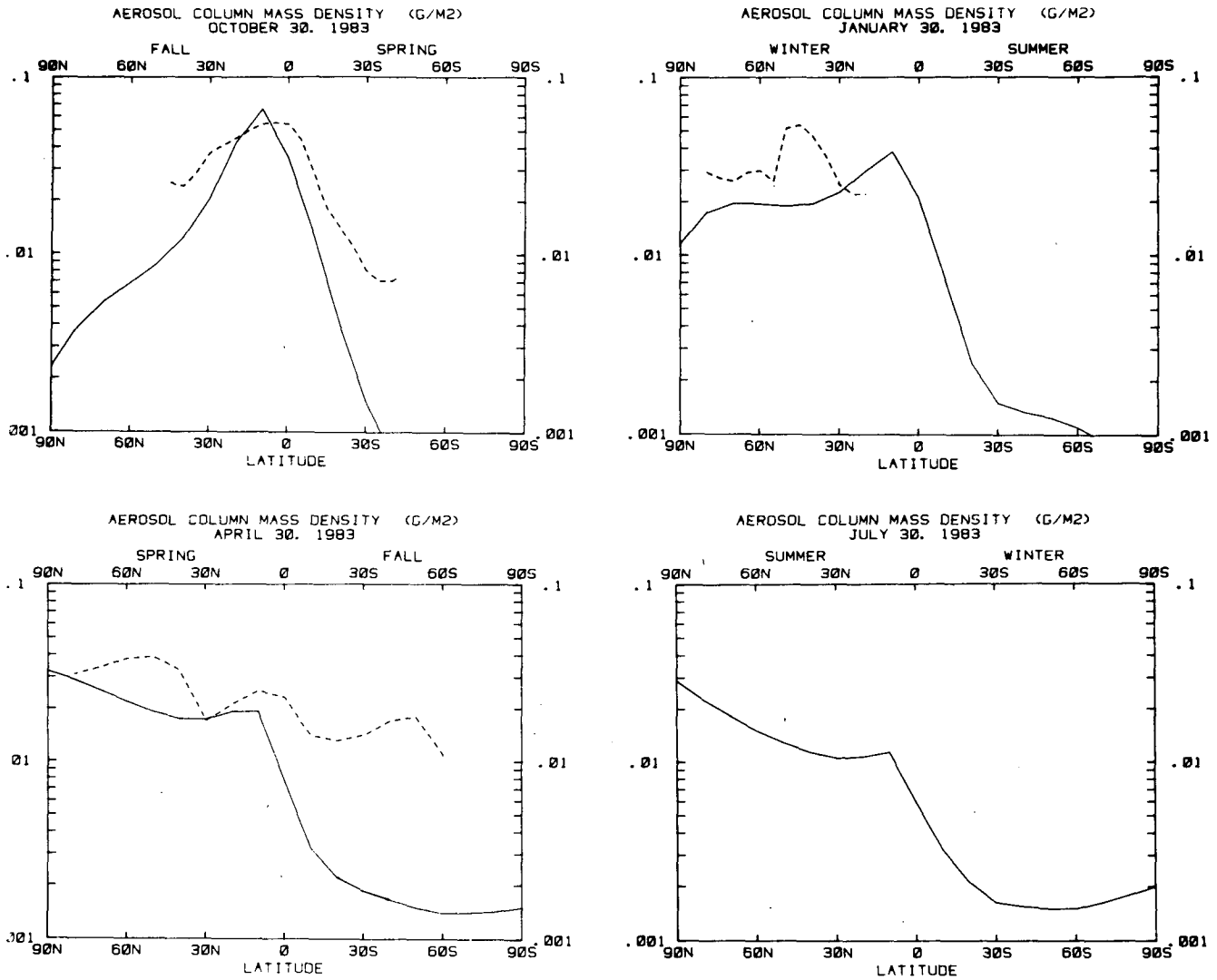

FIG. 9. Column mass density of the El Chichón aerosols as a function of latitude. Units are g m^{-2}. The four drawings refer to the same periods of time as in Fig. 8. Dashed lines refer to the estimates of McCormick et al. (1984).

measurements a much faster poleward motion during the 1982/83 winter. This is confirmed from data collected with different techniques and locations in the Northern Hemisphere. The transient character of this transport is confirmed from lidar measurements taken three months later during spring 1983 and from the rapid decrease of dust optical thickness measured at Mauna Loa during December 1982. This behavior is probably related to transient, sporadic stratospheric events that our 2D model is intrinsically unable to reproduce. Notice also that the apparent southward motion between January and April 1983 is due to lack of data in the southernmost latitudinal band in January.

Figure 9 shows the same kind of comparison but for the aerosol columnar density. While our results seem to agree reasonably well during October 1982, the comparison made in January 1983 reflects the mentioned fast poleward motion of the dust during that winter. The comparison made at the end of April 1983 shows the lack of mid latitude maxima in our model and the underestimation in the amount of dust in the Southern Hemisphere. On the other hand, the model seems to do a good job in the tropical region (and this will be confirmed from the Mauna Loa measurements).

Figures 10 and 11 show a comparison with lidar measurements taken at L'Aquila (42°N, 13°E). Figure 11 refers to extinction mixing ratios measured at $\lambda = 0.55$ μm. The extinction cross sections determined using a Mie scattering program with the calculated size distribution and for the appropriate refractive index (Palmer and Williams, 1975) are used to scale extinction mixing ratio and optical thickness in the model at the required wavelength. A remarkable agreement is found, except for a lower aerosol content shown by

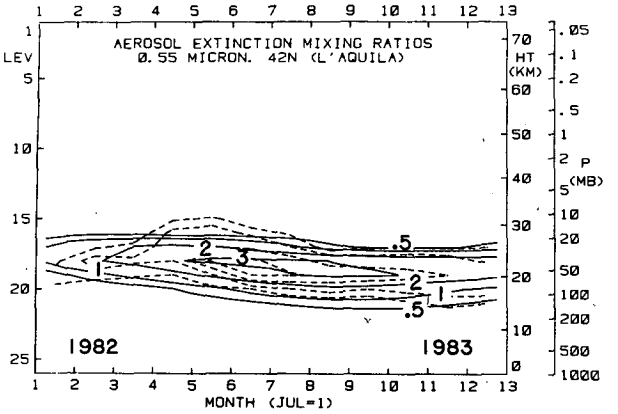

FIG. 10. Aerosol extinction mixing ratios at 0.55 μm as a function of altitude and time starting from July, 1982. Latitude is 42°N and dashed lines show the lidar measurements taken at L'Aquila (42°N, 13°E).

the model during the 1982/83 winter in the upper layers of the cloud. This is confirmed in Fig. 11 where we show the optical thicknesses between 20–30 and 10–20 km. Our model shows a clear underestimation of the dust optical depth in the upper layers of the cloud, particularly in the months of the 1982/83 winter season. This effect, apart from zonal asymmetries, could also be related to the increased lidar error for high altitude thin layers. However, the optical thickness reported by the measurements in the 20–30 km range is a considerable percentage of the total, so that the underprediction in the highest layers is actually reflected also in the totals. This is confirmed by the data taken at Garmisch, that in Fig. 12 and 13 are compared with the model results.

Figure 12 shows both the column mass density and the optical thickness, while Fig. 13 represents the extinction mixing ratios at 0.55 μ. This comparison apparently shows a considerable underprediction of our model. This can be seen especially in the comparison of the optical thickness and column mass density (Fig. 13). In this case the agreement is rather poor showing that the model results are underestimating the amount of dust. Note however that lidar data taken at Garmisch show values for the optical thickness much higher than those of D'Altorio and Visconti (1984) and Hirono et al. (1984) taken at 30°N.

Figure 14 shows a comparison with data of Hirono et al. (1984) taken at 33°N. These data refer to optical thickness between 13.5 and 28 km, which roughly cover all the dust in the period studied with the model. Notice that we have used the 42.8 sr value to convert the vertically integrated backscattering coefficient to optical thickness while Hirono et al. (1984) have used a factor of the order 100–130 sr. Our results compare reasonably well from late fall. On the same figure we have reported the data points taken at 30°N by McCormick and Osborn (1985a,b; 1986a,b). The airborne lidar data shows values much higher than those observed in Japan before October, 1983. This discrepancy would indicate that the dust distribution in latitude is not homogeneous but is still organized in large "chunks" which are being observed roughly at the same longitude of the eruption. The lidar signal at the same latitude, but at different longitude, is probably produced by relatively small "pieces" of the cloud being transported there. Such a situation cannot be reproduced with a zonally averaged model and some of the inconsistencies could be attributed to the different stations sampling a rather inhomogeneous distribution. On the other hand, assuming a correct intercomparison of lidar data, our results would indicate a smoother latitudinal gradient than observed.

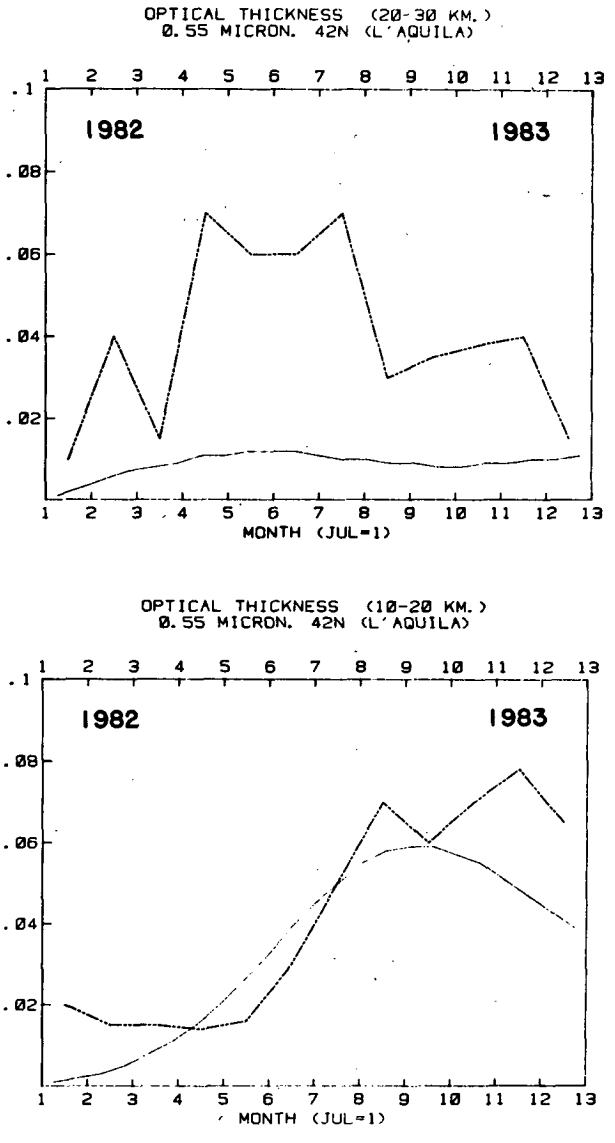

FIG. 11. Upper drawing shows the optical depth at 0.55 μm in the layer between 20 and 30 km. Lower drawing refers to the layer between 10 and 20 km. Latitude and time are the same as in Fig. 10. Dashed-dotted lines show the data from the lidar station of L'Aquila.

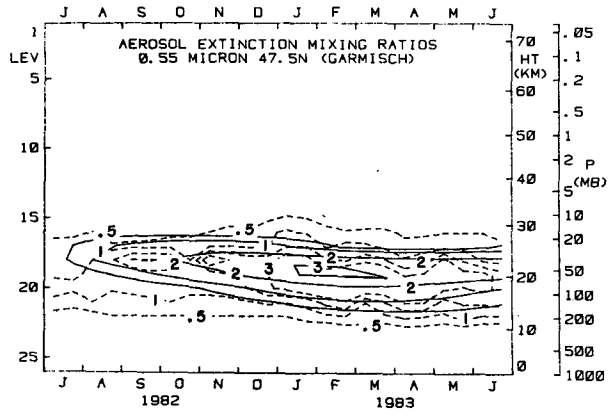

FIG. 12. Aerosol extinction mixing ratio at 0.55 μ as a function of altitude and time starting from July, 1982. Latitude is 47.5°N and dashed lines refer to lidar data taken at Garmisch.

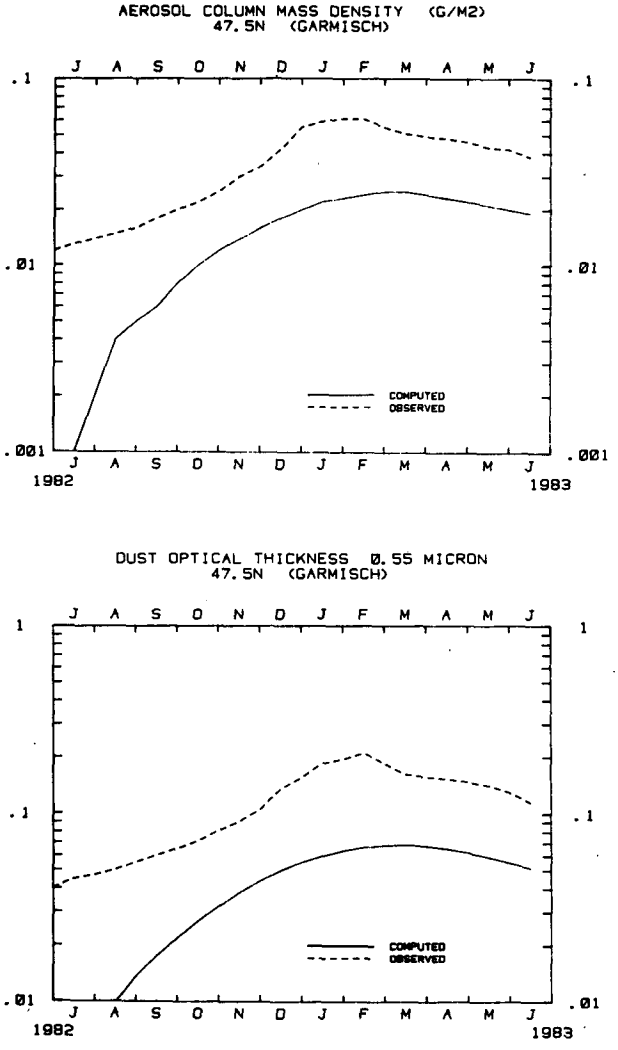

FIG. 13. Aerosol column mass density (upper figure) and optical thickness (lower figure) deduced from Garmisch data (dashed line) compared with model results (solid line).

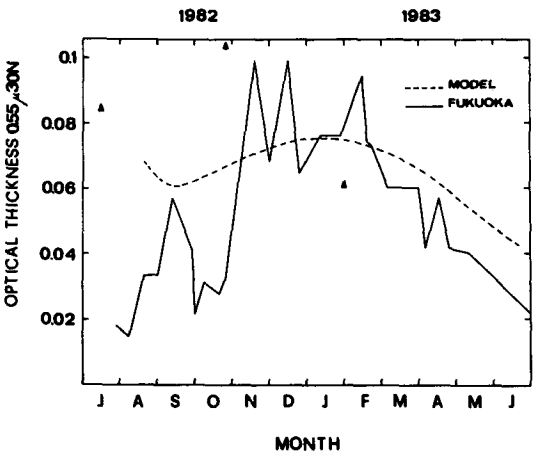

FIG. 14. The solid line shows optical thickness obtained from lidar data taken at Fukuoka (Japan) at 0.55 μ, at a latitude of 33°N. Data are compared to model results (dashed lines) for 30°N. Triangles are airborne lidar data from McCormick and Osborn (1985a,b; 1986a,b).

Figures 15 and 16 show a comparison of our results with the measurements taken at Mauna Loa (19°N, 156°W). Figure 15 shows the dust optical thickness above the tropopause at 0.55 μm (upper drawing) and the corresponding column mass density in g m^{-2} (lower drawing). Figure 16 shows the altitude where the maximum backscattering ratio is found (upper drawing) and the altitude where half optical thickness is reached (lower drawing). Dashed lines refer to the observed data (DeLuisi, personal communication, 1986), that have been redrawn in both figures. A good agreement is found, except for the initial columnar density that is higher in our model (90 mg m^{-2} against 66 mg m^{-2}). This is partially related to the altitude where the cloud center is found (see Fig. 14) and which is a little higher in the Mauna Loa data compared to the McCormick ones.

An important feature in the Mauna Loa data is the sharp decrease in the optical thickness during December 1982 and that should be related to the mentioned fast meridional transport that moved a large amount of dust toward mid-high latitudes.

5. Conclusions

A two-dimensional model of the atmosphere has been used to calculate aerosol transport from the El Chichón eruption. The results have been compared with a set of lidar data taken from stations at different latitudes and with an airborne lidar. The model uses the appropriate dynamics and climatology for the season in the appropriate hemisphere. The aerosol from a source located at about 15°N is slowly transported in both hemispheres but with a considerable degree of asymmetry. This results in a larger optical thickness over the Northern Hemisphere with respect to the Southern Hemisphere which is not shown in the lidar data. Also the build-up of the optical thickness over

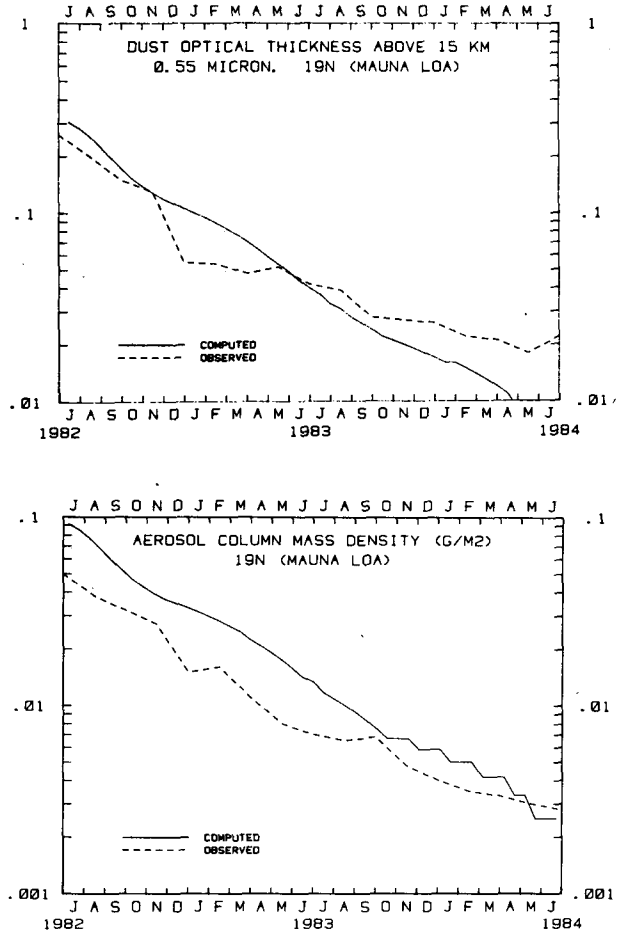

FIG. 15. Upper drawing shows the optical depth at 0.55 μm above 15 kilometers as a function of time. Lower drawing refers to the column mass density (g m^{-2}). Latitude is 19°N and the dashed lines show the results of lidar measurements taken at Mauna Loa (19°N, 156°W).

the poles, as results from the model, gives ten times as much aerosols over the Arctic with respect to the South Pole, while measurements give only a factor 2–5.

In the model the aerosols are considered as a passive tracer, that is nucleation, coagulation and condensation are neglected and the particles are subject to sedimentation only. This also turns out not to be a good assumption, at least at high altitudes where depletion at large sizes is observed in contradiction with experimental data. The depletion is also present in the results for the optical thickness especially above 20 km, where the model underpredicts the lidar data. At lower elevation the agreement is better for the calculated optical thickness (or mass) and should not be affected by the different size distribution because the backscattering coefficient is independent of size distribution at a fixed wavelength; at least for polydisperse particles with maximum radii of 1.5 μ (which is our case). Aerosol takes several months to reach middle latitude and during this time, in the model, sedimentation depletes the high altitude layers. A better approximation would be to include other microphysical processes, especially nucleation and coagulation, which is shown by the experimental data to continue to take place several months after the eruption.

Experimental latitudinal profiles of dust show a sudden decrease at middle-high latitude in the winter of 1982/83, which is not reproduced by the model. Both the pronounced asymmetry in the dust distribution and the inability to produce the sudden decrease are ascribed to the zonally averaged characteristic of the model: mixing resulting from discrete and sporadic events which the model is unable to simulate.

A particularly good fit is found for the equatorial station at Mauna Loa, which is roughly at the same latitude of the eruption.

From this numerical experiment we can draw several conclusions. Zonally averaged two dimensional models, although routinely used to calculate trace gases dis-

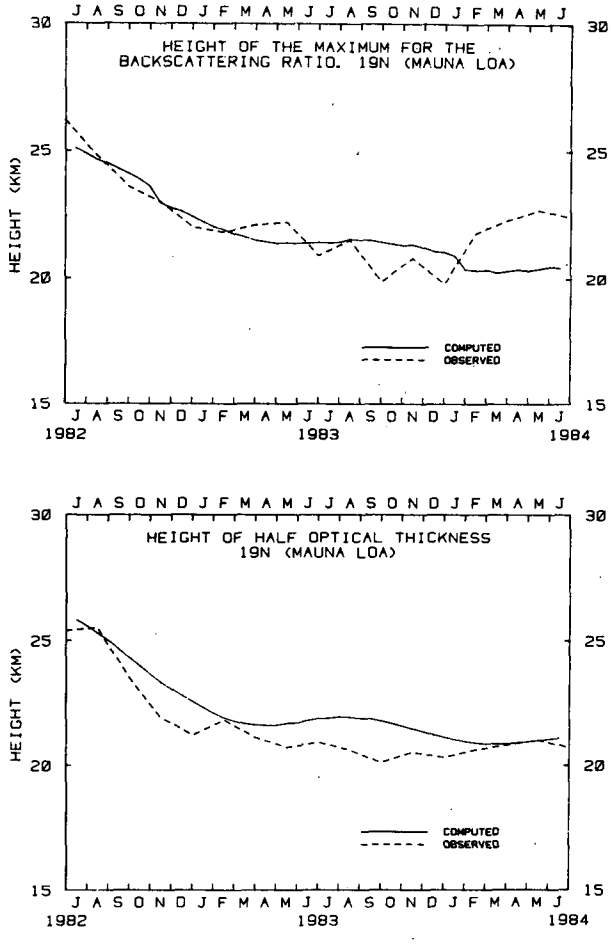

FIG. 16. Upper drawing shows the altitude of the maximum for the backscattering ratio as a function of time. Lower drawing refers to the altitude where half optical thickness is found. Latitude is the same as in Fig. 13. Dashed lines refer to the data taken at Mauna Loa.

tribution, should be used with caution when dealing with sporadic and transient events like volcanic eruption. The duration of the event is comparable with the averaging period and consequently this is not a good approximation.

Even several months after the eruption, aerosol can not be considered as a passive tracer so that coagulation or nucleation processes should be considered. This difficulty could be removed by including in the model heterogeneous chemistry and microphysical processes.

Acknowledgments. Special thanks are due to John DeLuisi who kindly provided prepublished data to one of the authors (G.P.) on the occasion of the first NATO Advanced School of Climatology (Erice, Italy, May 1986). This work is supported in part by Piano Spaziale Nazionale.

REFERENCES

Capone, L., O. B. Toon, R. C. Whitten, R. P. Turco, C. A. Reigel and K. Santhanam, 1983: A two-dimensional model simulation of the El Chichón volcanic eruption cloud. *Geophys. Res. Lett.*, **10,** 1053.

Cunnold, D., F. Alyea, N. Phillips and R. G. Prinn, 1975: A three-dimensional dynamical-chemical model of the atmospheric ozone. *J. Atmos. Sci.*, **32,** 170.

D'Altorio, A., and G. Visconti, 1984: Lidar monitoring at mid latitude of the stratospheric aerosol perturbation produced by the El Chichón eruption. *Geof. Int.*, **23,** 233.

Dunkerton, T. J., 1978: On the mean meridional mass motion of the stratosphere and mesosphere. *J. Atmos. Sci.*, **35,** 2325–2333.

Gille, J. C., L. V. Lyjak and A. K. Smith, 1987: The global circulation in the middle atmosphere for the Northern winter period. *J. Atmos. Sci.*, 1437–1451.

Hirono, M., T. Shibata, M. Fujiwara and N. Fujiwara, 1984: Enormous increase of volcanic clouds in the stratosphere over Fukouka after April 1982. *Geofis. Int.*, **23,** 259.

Holton, J. R., 1981: An advective model for two-dimensional transport of stratospheric trace species. *J. Geophys. Res.*, **86,** 11 989–11 994.

Hoffman, D. J., and J. M. Rosen, 1984: Balloonborne particle counter observations of the El Chichón aerosol layers in the 0.01–1.8 μm radius range. *Geofis. Int.*, **23,** 155–186.

Kida, H., 1983: General circulation of air parcels and transport characteristics derived from a hemispheric GCM, 1. A determination of advective mass flow in the lower stratosphere. *J. Meteor. Soc. Japan,* **61,** 171–187.

King, M. D., Harshvardhan and A. Arking, 1984: A model of the radiative properties of the El Chichón stratospheric aerosol layer. *J. Climate Appl. Meteor.*, **23,** 1121.

Labitzke, K., B. Naujokat and M. P. McCormick, 1983: Temperature effects on the stratosphere of the April 4, 1982 eruption of El Chichón, Mexico. *Geophys. Res. Lett.*, **10,** 24.

Lorenz, E., 1971: An *N*-cycle time differencing scheme for stepwise numerical integration. *Mon. Wea. Rev.*, **99,** 644–648.

McCormick, M. P., 1986: Presentation of SAM II and SAGE I results at the *Sixth Int. Symp. on Solar-Terrestrial Physics,* Toulouse, France.

——, and M. T. Osborn, 1985a: Airborne lidar measurements of El Chichón stratospheric aerosols, October 1982 to November 1982, NASA Ref. Publ. 1136.

——, and ——, 1985b: Airborne lidar measurements of El Chichón, January 1983 to February 1983, NASA Ref. Publ., 1148.

——, and ——, 1986a: Airborne lidar measurements of El Chichón stratospheric aerosols. July 1982, NASA Ref. Publ., 1166.

——, and ——, 1986b: Airborne lidar measurements of El Chichón, May 1983, NASA Ref. Publ., 1172.

——, and T. J. Swissler, 1983: Stratospheric aerosol mass and latitudinal distribution of the El Chichón volcanic eruption. *Geophys. Res. Lett.*, **10,** 27.

——, T. J. Swissler, W. H. Fuller, W. H. Hunt and M. T. Osborn, 1984: Airborne and ground-based lidar measurements of the El Chichón stratospheric aerosol from 90°N to 90°S. *Geofys. Int.*, **23,** 187–222.

——, and C. R. Trepte, 1986: Polar stratospheric optical depth observed by SAM II satellite instrument between 1978 and 1985, Preprint.

Palmer, K. F., and Williams, D., 1975: Optical constants of sulfuric acid; application to the cloud of Venus. *Appl. Optics,* **14,** 208.

Pinnick, R. G., S. G. Jennings and P. Chylek, 1980: Relationship between extinction, absorption, backscattering and mass content of sulfuric acid aerosols. *J. Geophys. Res.*, **85,** 4059–4066.

Pitari, G., and G. Visconti, 1980: A two-dimensional model of the distribution of trace gases in the stratosphere and troposphere. *Il Nuovo Cimento,* **3C,** 5, 541.

——, and ——, 1981: Two-dimensional simulation of volcanic dust transport and photochemical production and comparison with lidar data, presented at the ICACGP session, IAMAP, Hamburg 17–28 August.

——, and ——, 1985: Two-dimensional tracer transport: derivation of residual mean circulation and eddy transport tensor from a 3D model data set. *J. Geophys. Res.*, **90,** 8019.

——, M. Verdecchia and G. Visconti, 1987: A transformed Eulerian model to study possible effects of the El Chichón eruption on the stratospheric circulation. *J. Geophys. Res.*, **92,** 10961.

Plumb, A., 1987: Parcel dispersion in stratospheric models, in *Transport Processes in the Middle Atmosphere,* R. Garcia and G. Visconti, Eds., Reidel.

——, and J. D. Mahlman, 1987: The zonally-averaged transport characteristics of the GFDL general circulation/transport model. *J. Atmos. Sci.*, **44,** 298.

Pollack, J. B., and T. P. Ackerman, 1983: Possible effects of the El Chichón cloud on the radiative budget of northern tropics. *Geophys. Res. Lett.*, **10,** 1057.

——, O. B. Sagan, A. Summers, B. Baldwin and W. Van Camp, 1976: Volcanic explosions and climatic changes: a theoretical assessment. *J. Geophys. Res.*, **81,** 1071.

Solomon, S., J. T. Kiehl, R. R. Garcia and W. Grose, 1986: Tracer transport by the diabatic circulation deduced from satellite observations. *J. Atmos. Sci.* **43,** 1603–1617.

Swissler, T. J., M. P. McCormick and J. D. Spinhirne, 1983: El Chichón eruption cloud: comparison of lidar and optical thickness measurements for October 1982. *Geophys. Res. Lett.*, **10,** 9, 885–888.

Tung, K. K., 1983: Modeling of tracer transport in the middle atmosphere. *Dynamics of the Middle Atmosphere,* 412–444, Terra Scientific.

Turco, R. P., P. Hamill, O. B. Toon, R. C. Whitten and C. S. Kiang, The NASA-Ames Research Center, 1979: Stratospheric Aerosol Model. I. Physical Processes and Numerical Analogs. NASA TP-1362.

——, O. B. Toon, R. C. Whitten, P. Hamill and R. G. Keesee, 1983: The 1980 eruptions of Mount St. Helens: Physical and chemical processes in the stratospheric clouds. *J. Geophys. Res.*, **88,** 5299.

Visconti, G., and G. Pitari, 1987: Seasonal and latitudinal distribution of trace gases in the stratosphere: results from a 2D residual circulation model. *J. Atmos. Chem.*, **5,** 255–290.

——, A. Matarese and G. Pitari, 1987: A study of the El Chichón perturbation in the stratospheric dynamics: results from a 3D model. *Physica Scripta,* in press.